LETTERS
PUBLISHED ONLINE: 24 AUGUST 2014 | DOI: 10.1038/NNANO.2014.168
nature nanotechnology

Optomechanical coupling between a multilayer graphene mechanical resonator and a superconducting microwave cavity

V. Singh*, S. J. Bosman, B. H. Schneider, Y. M. Blanter, A. Castellanos-Gomez and G. A. Steele*

The combination of low mass density, high frequency and high quality factor, *Q*, of mechanical resonators made of two-dimensional crystals such as graphene[1–8] make them attractive for applications in force/mass sensing and exploring the quantum regime of mechanical motion. Microwave optomechanics with superconducting cavities[9–14] offers exquisite position sensitivity[10] and enables the preparation and detection of mechanical systems in the quantum ground state[15,16]. Here, we demonstrate coupling between a multilayer graphene resonator with quality factors up to 220,000 and a high-*Q* superconducting cavity. Using thermomechanical noise as calibration, we achieve a displacement sensitivity of 17 fm $Hz^{-1/2}$. Optomechanical coupling is demonstrated by optomechanically induced reflection and absorption of microwave photons[17–19]. We observe 17 dB of mechanical microwave amplification[13] and signatures of strong optomechanical back-action. We quantitatively extract the cooperativity *C*, a characterization of coupling strength, from the measurement with no free parameters and find *C* = 8, which is promising for the quantum regime of graphene motion.

Exfoliated two-dimensional crystals offer a unique platform for mechanics because of their low mass, low stress and high quality factors (Q). Following the initial demonstration of graphene mechanical resonators[1–3] there has been considerable progress in harnessing the mechanical properties of graphene for mass sensing[2], the study of nonlinear mechanics[5,6] and voltage-tunable oscillators[7,8]. Graphene is also potentially attractive for experiments with quantum motion, where the high quality factor[4,5] and low mass of graphene resonators result in large zero-point fluctuations over a small bandwidth. The high frequency of graphene resonators also provides low phonon occupation at cryogenic temperatures. Previously employed optical[1] and radiofrequency (RF) techniques[2,3,5,6] have enabled the detection and characterization of graphene resonators, but they did not provide a clear path towards the quantum regime.

A possible route to the ultimate limit in sensitivity is provided by cavity optomechanics[20], which is capable of detecting motion near and below the standard quantum limit[10,11]. It has also been used to bring mechanical systems into their quantum ground state with sideband cooling[15,21] and to entangle microwave photons with the motion of a mechanical resonator[16]. A natural candidate for implementing cavity optomechanics with graphene resonators is a high-Q superconducting microwave cavity. However, combining graphene with superconducting cavities in such a way that both retain their excellent properties (such as their high quality factors) is technologically challenging.

Here, we present a multilayer graphene mechanical resonator coupled to a superconducting cavity. Using a deterministic all-dry transfer technique[22] and a novel microwave coupling design, we are able to combine these two elements without sacrificing the exceptional intrinsic properties of either. Although multilayer graphene has a higher mass than a monolayer, it could be advantageous for coupling to a superconducting cavity because of its lower electrical resistance. Figure 1a,b presents optical and electron microscope images of the device. The superconducting cavity is a quarter-wavelength coplanar waveguide (CPW) resonator, which can be modelled by an effective lumped capacitance C_{sc} and inductance L_{sc}, with added capacitances from the graphene drum C_g and from the fixed coupling capacitor C_c to the feedline (as shown in Fig. 1c).

Figure 1d shows the measured reflection coefficient ($|S_{11}|$) of the cavity with low probe power at $T = 14$ mK. A fit of the amplitude and phase of the reflection coefficient yields a resonant frequency $\omega_c \approx 2\pi \times 5.9006$ GHz, external dissipation rate of $\kappa_e = 2\pi \times 188$ kHz and a total dissipation rate of $\kappa = 2\pi \times 242$ kHz. The coupling efficiency $\eta = \kappa_e/\kappa \approx 0.77$ (>1/2) indicates that the cavity is overcoupled (see Supplementary Section III for additional cavity characterization). Based on the designed impedance of the transmission line resonator ($Z_0 = 51\ \Omega$) and geometric capacitance of the graphene resonator ($C_g \approx 578$ aF), we estimate a cavity pull-in parameter of $G = \frac{d\omega_c}{dx} \approx 2\pi \times 26.5$ kHz nm^{-1}.

Figure 2 presents the characterization of the mechanical properties of the multilayer graphene resonator using a homodyne measurement scheme[9]. Here, the cavity is used as an interferometer to detect motion while injecting a microwave signal near ω_c and exciting the mechanical resonator with an a.c. voltage applied to the gate. Figure 2a shows the mechanical response of the multilayer graphene resonator. A Lorentzian lineshape fit yields a mechanical resonance frequency of $\omega_m \approx 2\pi \times 36.233$ MHz and a quality factor of $Q_m \approx 159{,}000$ at 14 mK. The mechanical resonance frequency is much larger than the cavity linewidth ($\omega_m/\kappa \approx 150$), placing the set-up in the sideband resolved limit, a prerequisite for ground state cooling. The cavity can also be used to detect undriven motion such as the thermomechanical noise of the drum, shown in the inset of Fig. 2a, corresponding to a mechanical mode temperature of 96 mK (see Supplementary Section V for additional details). The thermal motion peak serves as a calibration for the displacement sensitivity. While driving the cavity at resonance and utilizing its full dynamic range before electrical nonlinearity sets in (–41 dBm injected power) we estimate a displacement sensitivity for mechanical motion of 17 fm $Hz^{-1/2}$. Using a d.c. voltage applied to the gate electrode, the frequency of the multilayer graphene resonator can also be tuned (Fig. 2b). The decrease in resonance frequency ω_m for non-zero gate voltage is due to electrostatic softening of the spring constant as has been observed previously[3].

Figure 3 demonstrates optomechanical coupling between the multilayer graphene mechanical resonator and the cavity, mediated

Kavli Institute of NanoScience, Delft University of Technology, PO Box 5046, 2600 GA, Delft, The Netherlands. *e-mail: v.singh@tudelft.nl; g.a.steele@tudelft.nl

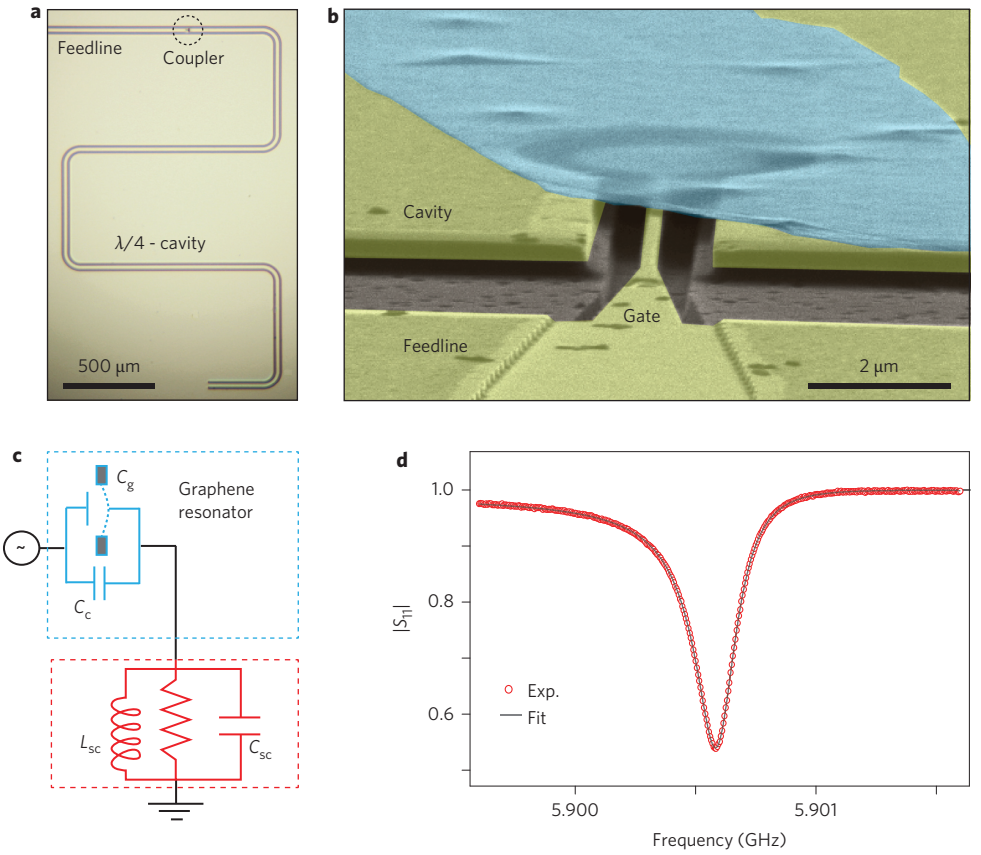

Figure 1 | Characterization of the superconducting cavity coupled to a multilayer graphene mechanical resonator. a, Optical image of a superconducting cavity in a quarter-wave coplanar waveguide geometry. Microwave photons are coupled in and out of the cavity via a feedline that is capacitively coupled to the coplanar waveguide centre conductor by a gate capacitor (coupler). **b**, This gate capacitor includes a small gate electrode that extends from the feedline into the coplanar waveguide centre conductor. The tilted angle scanning electron micrograph (false colour) near the coupler shows a 4-μm-diameter multilayer (10-nm-thick) graphene resonator (cyan) suspended 150 nm above the gate. **c**, Schematic lumped element representation of the device with equivalent lumped parameters of capacitance $C_{sc} \approx 415$ fF and inductance $L_{sc} \approx 1.75$ nH. **d**, Reflection coefficient $|S_{11}|$ of the superconducting cavity measured at $T = 14$ mK (red). The grey curve is a fit to the data, giving an internal quality factor of $Q_i \approx 107{,}000$ and loaded quality factor of $Q_L \approx 24{,}250$.

by radiation pressure forces. The measurements of the cavity shown in Fig. 3 are similar to those in Fig. 1d, but in the presence of a strong drive signal detuned from the cavity frequency. The frequency is chosen such that $\omega_d = \omega_c + \omega_m$ ($=\omega_c - \omega_m$), referred to as driving the blue (red) detuned mechanical sideband. Including this second detuned drive tone, the cavity response acquires a sharp peak (blue sideband, Fig. 3a) or a sharp dip (red sideband, Fig. 3b) centred at the cavity resonance frequency. The sharp peak in Fig. 3a when driving on the blue sideband corresponds to optomechanically induced reflection (OMIR) of microwave photons, the same phenomenon as optomechanically induced transparency (OMIT)[17–19], but now in a reflection geometry. In OMIT, an analogue of electromagnetically induced transparency (EIT) in atomic physics, a transparency window opens in the absorption resonance of the cavity due to optomechanical coupling to the mechanical resonator. Driving on the red sideband (Fig. 3b), the cavity shows a sharp dip in the reflectivity of the cavity, corresponding to a process of optomechanically induced absorption (OMIA)[14].

Qualitatively, reflection and absorption features in the cavity response can be understood as follows. Consider the case of blue detuned driving, as shown by the schematic in Fig. 3a. With a strong sideband drive signal (ω_d, blue arrow) and a weak probe signal (ω_p near ω_c, black arrow), the beat between the two microwave signals generates a radiation pressure force that oscillates at $\Omega \approx \omega_m$ (green arrow), schematically shown as process 1. This oscillating radiation force at frequency Ω coherently drives the graphene resonator. Mechanical motion of the graphene resonator in turn modulates the drive field, resulting in a field appearing at $\omega_d - \Omega$ ($=\omega_p$, pink arrow), schematically shown as process 2. Being a coherent process, the upconverted field appearing at ω_p has a definite phase relation with the probe field and can either interfere constructively or destructively to produce OMIR or OMIA features in the cavity response. In contrast to the first observation of OMIT[18] and other configurations[12,23], here we observe OMIR on the blue sideband instead of the red sideband, a consequence of an overcoupled cavity ($\eta > 0.5$) (see Supplementary Section VII for a detailed discussion).

Using radiation pressure to drive the motion, we can characterize the resonator at $V_g = 0$ V, which is otherwise inaccessible with electrostatic driving. Using OMIA, we find quality factors as high as $Q_m \approx 220{,}000$ at $V_g = 0$ V, the highest detected for a graphene resonator (for additional data see Supplementary Section VII). Inside the OMIA window there is a fast change in the phase response of the microwave signal[19,23]. This can be used to implement a microwave photon storage device using a mechanical resonator (for additional data see Supplementary Section VII). For the present device we estimate a storage time of 10 ms, comparable in magnitude to that recently demonstrated in conventional mechanical resonators[23]. However, the group delay observed here using OMIA occurs in a very narrow bandwidth, set roughly by the mechanical linewidth, together with significant optomechanical absorption losses.

In Fig. 4, we explore the optomechanical interaction with the multilayer graphene resonator for stronger coupling. The

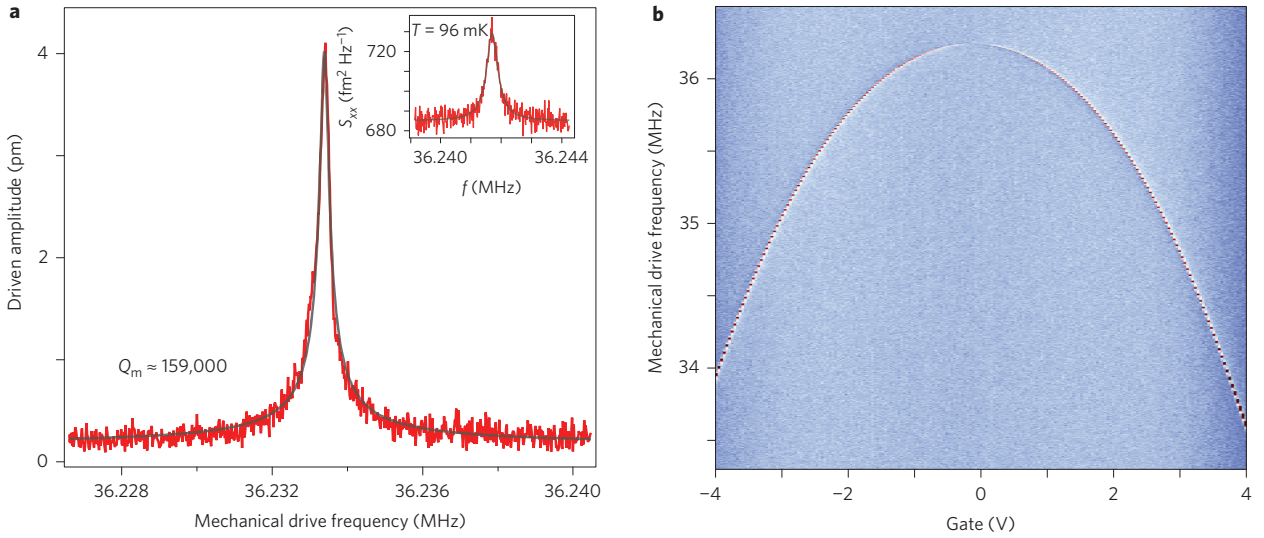

Figure 2 | Sideband resolved detection of the motion. a, Driven response of the multilayer graphene resonator at $V_g = 150$ mV (red curve) at $T = 14$ mK. A Lorentzian fit (grey curve) to the response gives the mechanical quality factor $Q_m \approx 159{,}000$, corresponding to a mechanical dissipation rate of $\gamma_m \approx 2\pi \times 228$ Hz. A mechanical frequency of $\omega_m \approx 2\pi \times 36.233$ MHz and cavity linewidth of $\kappa = 2\pi \times 242$ kHz imply a sideband resolved limit ($\omega_m \gg \kappa$). Inset: displacement spectral density S_{xx} due to thermal noise measured with mechanical mode thermalized at $T = 96$ mK. The thermal peak corresponds to (27 fm Hz$^{-1/2}$)^2. **b**, Colour-scale plot of the homodyne signal with mechanical drive frequency and gate voltage. The sharp change in colour represents the resonance frequency of the graphene resonator, indicating its negative tunability with gate voltage. At large gate voltages the response becomes nonlinear due to an increased driving force, which scales linearly with d.c. gate voltage. As the electromechanical driving force ($F_{ac} = \frac{dC_g}{dx} V_{ac} V_g$) vanishes at zero gate voltage, the measured signal disappears near $V_g = 0$ V.

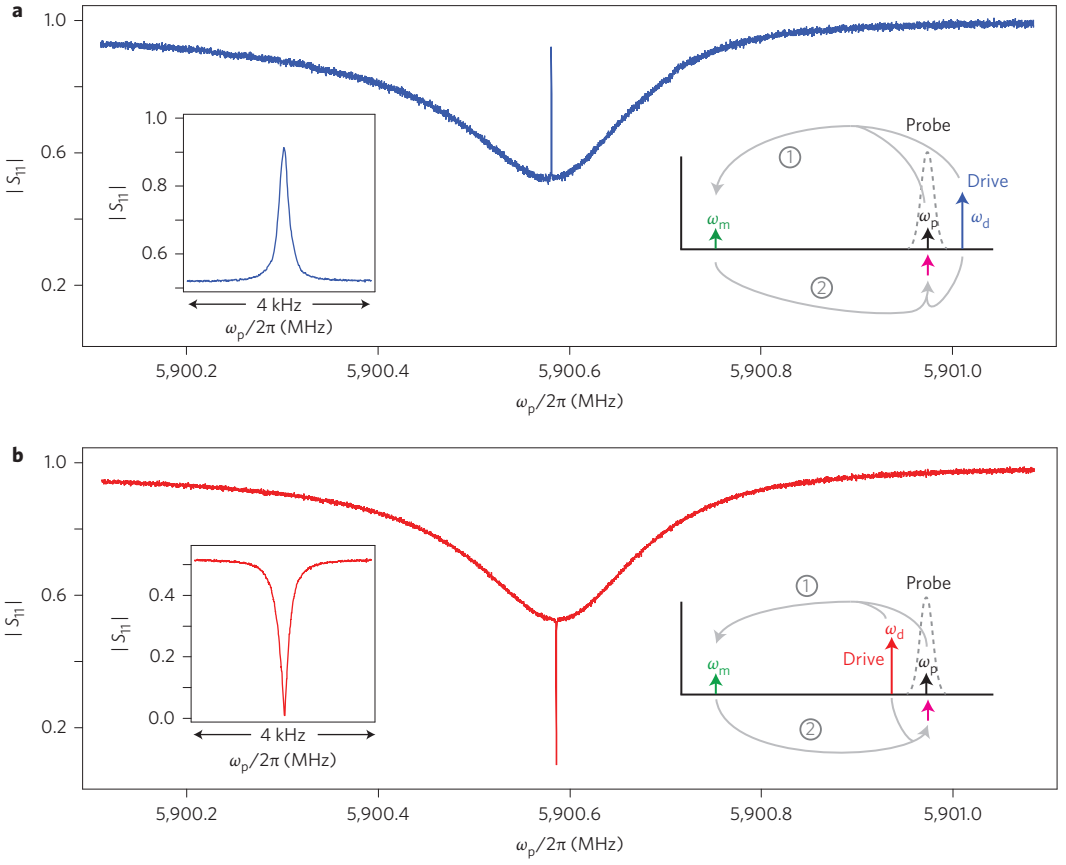

Figure 3 | Optomechanically induced absorption (OMIA) and optomechanically induced reflection (OMIR). Measurement of the cavity reflection $|S_{11}|$ in the presence of sideband detuned drive tone at $V_g = 0$ V. **a**, A blue detuned drive results in a window of OMIR in the cavity response. Inset: zoomed view of the OMIR window. **b**, A red detuned sideband drive opens an OMIA feature in the cavity response. Inset: zoomed view of the OMIA. Schematics in **a** and **b** illustrate the OMIR and OMIA features in terms of the interference of the probe field (black arrow) with the microwave photons, which are cyclically down and then upconverted by the optomechanical interaction (pink arrow).

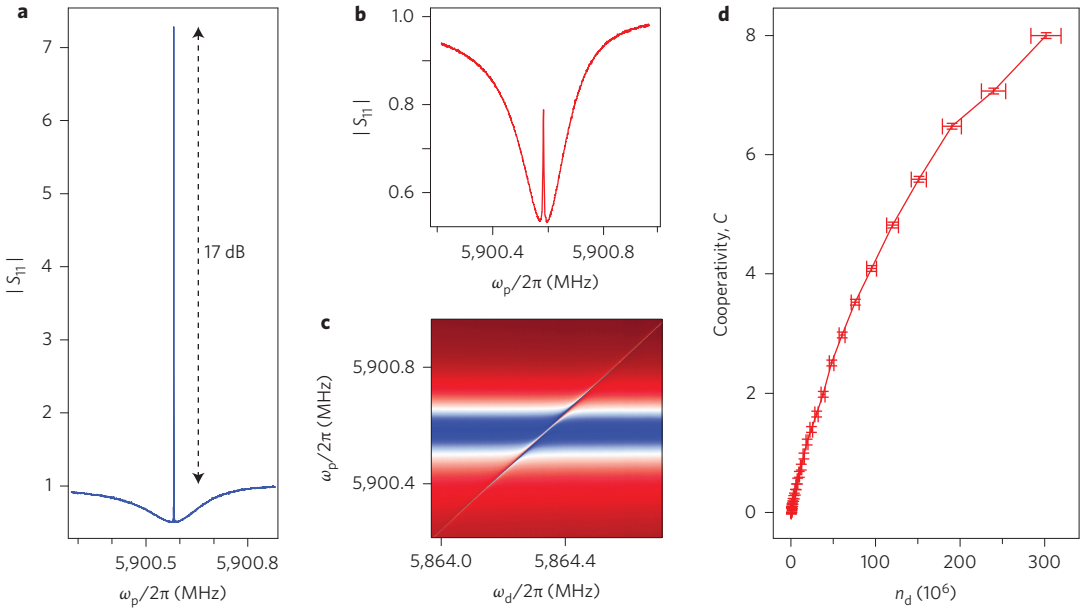

Figure 4 | Large cooperativity with a multilayer graphene mechanical resonator. a, Measurement of the cavity reflection $|S_{11}|$ under a strong blue detuned drive ($n_d \approx 1.5 \times 10^7$). At the centre of the cavity response, the reflection coefficient exceeds 1, corresponding to mechanical microwave amplification of 17 dB by the graphene resonator. **b**, Measurement of the cavity reflection $|S_{11}|$ under a strong red detuned drive ($n_d \approx 3 \times 10^8$). With strong red detuned drive, the optomechanically induced absorption feature becomes optomechanically induced reflection and we observe the onset of the normal mode splitting, also visible in the colourscale plot in **c** as an avoided crossing while sweeping the drive frequency across the red sideband. The sweep measurement was performed with constant drive power. **d**, Plot of cooperativity C versus number of red detuned photons n_d, in which we obtained $C = 8$. Horizontal error bars result from the statistical uncertainty in determining the single-photon coupling strength (g_0), dissipation rate (κ) and mechanical dissipation rate (γ_m).

optomechanical coupling strength g is tunable by the number of drive photons inside the cavity (n_d) as $g = Gx_{zpf}\sqrt{n_d} = g_0\sqrt{n_d}$, where x_{zpf} is the amplitude of the quantum zero-point fluctuations of the mechanical resonator and g_0 is the single-photon coupling strength[20]. We calibrate g_0 using a frequency modulation scheme[23,24] (for additional data see Supplementary Section VI) and find $g_0 = 2\pi \times 0.83$ Hz. The combination of the calibration of g_0 and the OMIA data allows the absolute calibration of the photon number in the cavity. Figure 4a shows the cavity response while driving on the blue sideband with $n_d \approx 1.5 \times 10^7$. Compared to the reflection feature shown in Fig. 3a, the OMIR peak has increased such that the reflection coefficient now exceeds unity, indicating more probe photons are coming out than we are putting in. This gain of microwave photons arises from mechanical microwave amplification[13] by the graphene resonator. We achieve up to ~17 dB gain in a bandwidth of ~300 Hz with added noise photons that, theoretically, can be as low as the number of thermal phonons ($\bar{n}_{th}$) in the mechanical resonator[13]. Increasing the blue detuned drive further leads to self-oscillation of the mechanical resonator. The origin of microwave amplification can also be understood in terms of the optomechanical backaction on the cavity: when the coupling strength becomes sufficiently strong such that $4g^2/\gamma_m$ overcomes the internal dissipation rate of the cavity (κ_i), the net effective internal damping rate of the microwave cavity becomes negative.

Figure 4b shows the cavity response for a red detuned drive with $n_d \approx 3 \times 10^8$. In contrast to Fig. 3b, the absorption feature has become a reflection (transparency) window. This crossover occurs when the optomechanical coupling becomes sufficiently strong that the effective internal dissipation rate of the cavity $\kappa_i^{eff} = \kappa_i + \frac{4g^2}{\gamma_m}$ exceeds the external dissipation rate κ_e. The reflection window in Fig. 4b is considerably greater in width than the one in Fig. 3a. This is an indication of optomechanical backaction. Similar to the modification of the internal dissipation rate of the cavity, the mechanical dissipation rate γ_m is also modified, $\gamma_m^{eff} = \gamma_m(1 + \frac{4g^2}{\kappa\gamma_m})$, leading to broadening of the OMIR feature and onset of the normal mode splitting of the cavity resonance[12,25]. At the highest photon numbers we achieve $2g/\kappa \approx 0.12$, corresponding to 12% of the strong coupling limit. At these coupling rates, a weak avoided crossing in the cavity response can be seen when a detuned drive is swept across the red sideband (Fig. 4c).

A useful feature of OMIA–OMIR data is that the height of the peak or depth of the dip allows one to extract $4g^2/\kappa\gamma_m \equiv C$, the optomechanical cooperativity, with no free parameters. The cooperativity C is an important characterization for optomechanical experiments. For example, in the sideband resolved limit, the criterion for cooling the mechanical resonator to its quantum ground state is $C + 1 > \bar{n}_{th}$, where $\bar{n}_{th}$ is the number of thermally excited quanta in the resonator[20]. Figure 4d shows the cooperativity of our device extracted from the OMIA data as a function of the number of red detuned drive photons inside the cavity (n_d). Increasing n_d, we have been able to achieve $C = 8$. The value of C should scale with n_d, but in our device the intrinsic mechanical quality factor begins to decrease at higher cavity powers, leading to a deviation from the linear relation (see Supplementary Section VII for detailed characterization). With $C = 8$, we achieve a maximum multiphoton coupling strength of $g \approx 2\pi \times 14$ kHz, with $n_d \approx 3 \times 10^8$.

We conclude by discussing the future prospects of the optomechanical device presented here. In principle, assuming equilibrium with the phonon bath at 14 mK, the cooperativity achieved here brings the system close to the quantum coherent regime $C \approx \bar{n}_{th} = \frac{k_B T}{\hbar\omega_m}$. In practice, however, a higher margin on cooperativity is desired in order to overcome considerations such as technical noise or mode heating at high powers. Our estimates suggest that $C/\bar{n}_{th}$ will scale strongly with area, indicating that significant gains can be made with larger-area drums (see Supplementary Information). Quantum applications aside, using our graphene optomechanical device we have demonstrated 17 dB microwave

amplification, the potential for microwave photon storage for up to 10 ms, and the observation of a record-high mechanical quality factor of $Q_m \approx 220{,}000$ for a crystalline multilayer graphene resonator using radiation pressure force driving. As a detector, our cavity offers a displacement sensitivity of 17 fm $Hz^{-1/2}$ with a bandwidth three orders of magnitude larger than the mechanical dissipation rate ($\kappa/\gamma_m \approx 10^3$). This provides an unprecedented new tool for studying phenomena such as nonlinear restoring forces, nonlinear damping and mode coupling in graphene. Finally, the combination of our microwave design and transfer technique for resonator fabrication can be easily extended to other exfoliated two-dimensional crystals, including superconducting materials such as $NbSe_2$, potentially eliminating any resistive losses in the coupled optomechanical system.

Methods

A Mo/Re alloy was used to fabricate the superconducting cavity. Its large superconducting transition temperature ($T_c \approx 8$ K) allowed the achievement of a large dynamic range for the cavity. To fabricate the quarter-wavelength superconducting cavity in a coplanar waveguide geometry, the intrinsic Si substrate was first cleaned with hydrofluoric acid. The substrates were immediately loaded for sputtering and a layer of 300 nm Mo/Re was deposited. Following standard electron-beam lithography (EBL) and reactive-ion etching procedures, a quarter-wavelength cavity was etched. The gate was thinned in a second etch step so that it lay 150 nm below the surface of the CPW centre conductor metal. In the last step of fabrication, a multilayer graphene flake (thickness, ~10 nm) was transferred over the hole to form a capacitor between the superconducting CPW resonator and the feedline.

In this scheme, the motion of graphene dispersively modulates the cavity frequency ω_c through the change in C_g: $\omega_c(x) = 1/\sqrt{L_{sc}(C_{sc} + C_c + C_g(x))}$. (Note that the motion of graphene capacitor will also modulate the linewidth of the cavity, which is known as dissipative coupling. This was proposed recently to enable some novel optomechanical phenomena[25,26]. In our design, the dissipative coupling is significantly weaker than the dispersive coupling and will be neglected. Additional details are provided in the Supplementary Section II.) The use of the feedline capacitance to couple to the graphene resonator has some convenient practical advantages. In particular, d.c. gate voltages (to tune the mechanical frequency) and low-frequency RF voltages (to electrostatically drive the mechanical resonator) can easily be applied to the microwave feedline without spoiling the quality factor of the superconducting cavity.

Received 21 February 2014; accepted 16 July 2014; published online 24 August 2014

References

1. Bunch, J. S. *et al.* Electromechanical resonators from graphene sheets. *Science* **315,** 490–493 (2007).
2. Chen, C. *et al.* Performance of monolayer graphene nanomechanical resonators with electrical readout. *Nature Nanotech.* **4,** 861–867 (2009).
3. Singh, V. *et al.* Probing thermal expansion of graphene and modal dispersion at low-temperature using graphene nanoelectromechanical systems resonators. *Nanotechnology* **21,** 165204 (2010).
4. Barton, R. A. *et al.* High, size-dependent quality factor in an array of graphene mechanical resonators. *Nano Lett.* **11,** 1232–1236 (2011).
5. Eichler, A. *et al.* Nonlinear damping in mechanical resonators made from carbon nanotubes and graphene. *Nature Nanotech.* **6,** 339–342 (2011).
6. Song, X. *et al.* Stamp transferred suspended graphene mechanical resonators for radio frequency electrical readout. *Nano Lett.* **12,** 198–202 (2012).
7. Barton, R. A. *et al.* Photothermal self-oscillation and laser cooling of graphene optomechanical systems. *Nano Lett.* **12,** 4681–4686 (2012).
8. Chen, C. *et al.* Graphene mechanical oscillators with tunable frequency. *Nature Nanotech.* **8,** 923–927 (2013).
9. Regal, C. A., Teufel, J. D. & Lehnert, K. W. Measuring nanomechanical motion with a microwave cavity interferometer. *Nature Phys.* **4,** 555–560 (2008).
10. Teufel, J. D., Donner, T., Castellanos-Beltran, M. A., Harlow, J. W. & Lehnert, K. W. Nanomechanical motion measured with an imprecision below that at the standard quantum limit. *Nature Nanotech.* **4,** 820–823 (2009).
11. Rocheleau, T. *et al.* Preparation and detection of a mechanical resonator near the ground state of motion. *Nature* **463,** 72–75 (2010).
12. Teufel, J. D. *et al.* Circuit cavity electromechanics in the strong-coupling regime. *Nature* **471,** 204–208 (2011).
13. Massel, F. *et al.* Microwave amplification with nanomechanical resonators. *Nature* **480,** 351–354 (2011).
14. Hocke, F. *et al.* Electromechanically induced absorption in a circuit nano-electromechanical system. *New J. Phys.* **14,** 123037 (2012).
15. Teufel, J. D. *et al.* Sideband cooling of micromechanical motion to the quantum ground state. *Nature* **475,** 359–363 (2011).
16. Palomaki, T. A., Teufel, J. D., Simmonds, R. W. & Lehnert, K. W. Entangling mechanical motion with microwave fields. *Science* **342,** 710–713 (2013).
17. Agarwal, G. S. & Huang, S. Electromagnetically induced transparency in mechanical effects of light. *Phys. Rev. A* **81,** 041803 (2010).
18. Weis, S. *et al.* Optomechanically induced transparency. *Science* **330,** 1520–1523 (2010).
19. Safavi-Naeini, A. H. *et al.* Electromagnetically induced transparency and slow light with optomechanics. *Nature* **472,** 69–73 (2011).
20. Aspelmeyer, M., Kippenberg, T. J. & Marquardt, F. Cavity optomechanics. Preprint at http://arXiv.org/abs/1303.0733. Accepted in *Rev. Mod. Phys.* (2014).
21. Chan, J. *et al.* Laser cooling of a nanomechanical oscillator into its quantum ground state. *Nature* **478,** 89–92 (2011).
22. Castellanos-Gomez, A. *et al.* Deterministic transfer of two-dimensional materials by all-dry viscoelastic stamping. *2D Materials* **1,** 011002 (2014).
23. Zhou, X. *et al.* Slowing, advancing and switching of microwave signals using circuit nanoelectromechanics. *Nature Phys.* **9,** 179–184 (2013).
24. Gorodetsky, M. L., Schliesser, A., Anetsberger, G., Deleglise, S. & Kippenberg, T. J. Determination of the vacuum optomechanical coupling rate using frequency noise calibration. *Opt. Express* **18,** 23236–23246 (2010).
25. Weiss, T., Bruder, C. & Nunnenkamp, A. Strong-coupling effects in dissipatively coupled optomechanical systems. *New J. Phys.* **15,** 045017 (2013).
26. Elste, F., Girvin, S. M. & Clerk, A. A. Quantum noise interference and backaction cooling in cavity nanomechanics. *Phys. Rev. Lett.* **102,** 207209 (2009).

Acknowledgements

The authors thank A. Clerk for providing initial theoretical input. This work was supported by the Dutch Organization for Fundamental Research on Matter (FOM) and the Netherlands Organization for Scientific Research (NWO). A.C.G. acknowledges financial support through the FP7-Marie Curie project PIEF-GA-2011-300802 ('STRENGTHNANO').

Author contributions

V.S., S.B. and B.S. optimized and fabricated the quarter-wavelength superconducting cavity samples. A.C.G. developed the deterministic transfer method. V.S. and A.C.G. transferred graphene onto the superconducting cavity samples. V.S. and S.B. set up the low-temperature microwave measurement set-up. V.S. performed the measurement. Y.B. provided theoretical support. G.A.S. conceived the experiment and supervised the work. All authors contributed to writing the manuscript and provided critical comments.

Additional information

Supplementary information is available in the online version of the paper. Reprints and permissions information is available online at www.nature.com/reprints. Correspondence and requests for materials should be addressed to V.S. and G.A.S.

Competing financial interests

The authors declare no competing financial interests.